Supporting Information

Nitrogen-rich Porous Organic Cages with High Acetylene Storage and Separation Performance

Lijuan Feng,[ab] Yifei Xie,[a] Wenjing Wang,[a] Kongzhao Su*[ac] and Daqiang Yuan*[ac]

[a]*State Key Laboratory of Structural Chemistry, Fujian Institute of Research on the Structure of Matter, Chinese Academy of Sciences, Fuzhou, 350002, China*

[b]*College of Chemistry, Fuzhou University, Fuzhou 350116, China.*

[c]*University of the Chinese Academy of Sciences, Beijing, 100049, China*

E-mail: skz@fjirsm.ac.cn; ydq@fjirsm.ac.cn

Section S1. General Materials and Measurements

Bis(5-amino-1,2,4-triazol-3-yl)methane (BATM)[S1] and tetraformylcalix[4]resorcinarene (CR4ACHO)[S2] were synthesized by literature procedures, while other reagent-grade chemicals from commercial sources were employed without further purification. Fourier-transform infrared (750FT-IR) spectra were recorded with KBr pellets in the range of 4000 to 400 cm^{-1} under ambient conditions by using a Magna 750 FT-IR instrument from Bruker. ^1H NMR spectra were obtained with a Bruker Avance II 400 WB 400 MHz spectrometer equipped with a 4 mm double-resonance MAS probe and a spinning frequency of 8 kHz. Thermogravimetric analysis (TGA) was performed with a NETZSCH STA 449C thermal analyzer at a rate of 10°C min^{-1} under a nitrogen atmosphere in the range of 30 to 800°C. Powder X-ray diffraction (PXRD) patterns were collected in the 2θ range of 4 to 40° at a scanning rate of 1° min^{-1} with Cu Kα radiation (λ = 1.54 Å) by using a Rigaku-Dmax 2500 diffractometer. Simulation of the PXRD spectrum patterns is carried out by the single-crystal data and diffraction-crystal module of the *Mercury* program available free of charge via Internet at http://www.ccdc.cam.ac.uk/products/mercury/.

All the gas adsorption-desorption measurements of **CPOC-107** and **CPOC-203** were carried out by using an automatic volumetric adsorption equipment (Micromeritics, ASAP2020). Adsorbent characterizations N_2 adsorption/desorption isotherms were obtained at 77 K on the Micrometrics ASAP 2020 surface area and porosimetry analy-zer. Pore size distribution data were obtained from the N_2 sorption isotherms at liquid nitrogen temperature based on the DFT model in the Micromeritics ASAP 2020 software package (assuming cylinder pore geometry). The calculated pore volume and the micropore volume are based on the ASAP 2020 physisorption analyzer's built-in software. Prior to the adsorption analyses, the samples were evacuated at 373 K for 10h**.** The C_2H_2 and CO_2 gas sorption isotherms of **CPOC-107** and **CPOC-203** were measured at 273 K and 298 K. The experimental isotherm data for pure CO_2 and C_2H_2 were fitted using a dual Langmuir-Freundlich (L-F) model. The zero-coverage isosteric heats (Qst) of adsorption for C_2H_2 and CO_2 were calculated by utilizing the Clausius–Clapeyron equation based on fitting the dual-site Langmuir model using Equation 1, The parameters that were obtained from the fitting of the C_2H_2 and CO_2 adsorption isotherms can be found in Fig.s S11-S14. At the same time, in order to evaluate the material's ability to separate C_2H_2 and CO_2,the selectivity values for binary gas mixtures (50:50 v/v) of C_2H_2 /CO_2 calculated by IAST are depicted following Equation 2. (At equations: where *N* is the amount adsorbed, *R* is the universal gas constant, and x_{A} and x_{B} represent the equilibrium adsorption capacity of component A and component B, y_{A} and y_{B} represent the molar ratio of component A and component B in the original mixed gas.)

$$Q_{st} = -R\sum_{i=0}^{m} a_i N^i \qquad \textbf{(Equation 1)}$$

$$S_{A/B} = \frac{x_A y_B}{x_B y_A} \qquad \textbf{(Equation 2)}$$

In order to evaluate the separation performance for C_2H_2/CO_2, we used the Ideal Adsorbed Solution Theory (IAST) of Myers and Prausnitz[3] along with the pure component isotherm fits by dual-site Langmuir-Freundlich equation to determine the molar loadings in the mixture for specified partial pressures in the bulk gas phase (Equation 3). Where *N* is molar loading of species (mmol g^{-1}), *A* is saturation capacity of species (mmol g^{-1}), *B* is Langmuir constant (kPa^{-c}), *C* is Freundlich constant, and *P* is bulk gas phase pressure of species (kPa). The adsorption selectivity based on IAST for mixed C_2H_6/C_2H_4 is defined by the following equation 4.

$$N = A_1\frac{B_1\times P^{C_1}}{1+B_1\times P^{C_1}} + A_2\frac{B_2\times P^{C_2}}{1+B_2\times P^{C_2}} \qquad \textbf{(Equation 3)}$$

$$S_{A/B} = \frac{x_A y_B}{x_B y_A} \qquad \textbf{(Equation 4)}$$

$C_2H_2(1)/CO_2(2)$ mixture separations are envisaged to be carried out in fixed bed adsorbers. In such devices, the separations are dictated by a combination of adsorption selectivity and uptake capacity. Using the shock wave model for fixed bed adsorbers, Krishna[4, 5] has suggested that the appropriate metric is the separation potential (Δq) is determined as:

$$\Delta q = q_1\frac{y_{20}}{y_{10}} - q_2$$

In which y_{10}, y_{20} are the mole fractions of the feed mixture during the adsorption cycle. In the derivation of equation, it is assumed that the concentration "fronts" traversed the column in the form of shock waves during the desorption cycle. The molar loadings q_1, q_2 of the two components are determined using the Ideal Adsorbed Solution Theory (IAST) of Myers and Prausnitz using the unary isotherm fits as data inputs.[6] The physical significance of Δq is the maximum productivity of pure $C_2H_4(2)$ that is achievable in the adsorption cycle of PSA operations.

The penetration experiments were carried out on a self-built gas penetration device. The gas mixture flows through a column of samples containing different adsorbed substances and the composition of the gas at the outlet is continuously monitored by a mass spectrometer. A stainless steel column (2 mm in diameter, 110 mm in length) was used to carry the samples. First, about 30 mg of silicon wool was weighed and the mass of the clean stainless steel column was recorded. Fill the steel column with 260 mg sample powder and plug the steel column with the remaining silicon wool. After loading the sample, connect the stainless steel column to the gas penetration device, open the helium valve (10 mL/min), and heat the sample at 100°C for about 12 h with the heating belt. The stainless-steel column is cooled to room temperature before the gas penetration test is performed. To test, turn off neon and open the C_2H_2/CO_2 mixture to flow through the sample column until the concentrations of C_2H_2 and CO_2 at the outlet are consistent with the mixing ratio concentration. The sample was regenerated by heating the sample at 100 ℃ under neon flow (10 mL/min) for 10 h between each test interval.

On the basis of the mass balance, the gas adsorption capacities can be determined as follows:

$$q_i = \frac{C_i V}{22.4 \times m} \times \int_0^t \left(1 - \frac{F}{F_0}\right) dt$$

Where qi is the equilibrium adsorption capacity of gas i (mmol g^{-1}), C_i is the feed gas concentration, V is the volumetric feed flow rate (cm^3 min^{-1}), t is the adsorption time (min), F_0 and F are the inlet and outlet gas molar flow rates, respectively, and m is the mass of the adsorbent (g).

The initial binding sites for C_2H_2 and CO_2 were determined from simulated annealing calculations using Adsorption Locator Module in the Material Studio program package. The possible main adsorption sites for adsorbed C_2H_2 and CO_2 molecules in the optimized **CPOC-107** and **CPOC-203** were investigated by the Dmol^3 module in the Material Studio program package. The PBE-type exchange-correlation functional with a generalized gradient approximation and the Double Numerical plus polarization (DNP) basis sets that include a d-type polarization function on all non-hydrogen atoms and a p-type polarization function on all hydrogen atoms were employed for all calculations. The FINE quality mesh size was employed in the calculations. During the gas-Cage structure optimization, the atomic positions of the **CPOC-107** and **CPOC-203** were kept immobile and the related single gas molecule was allowed to move during optimization. The adsorption energies were calculated in terms of the equation:

$$\Delta E = E_{POC+gas} - E_{POC} - E_{gas}$$

where $E_{POC+gas}$ stands for the energy of the optimized adsorbate-Cage structure, and E_{POC}, and E_{gas} denote the energies of the bare Cage structure and the isolated gas molecule, respectively. According to this equation, more negative adsorption energy means more favorable binding.

Section S2. Synthetic Procedures and Characterizations

Synthesis of CPOC-107: C4RACHO (0.05 mmol, 41 mg) and BATM (0.1 mmol, 19.7mg) were dissolved in 3 mL dimethyl sulfoxide. The mixture was sealed in a 10 mL glass vial, and put in an oven with a temperature of 100 °C for 72 hours without stirring, during which red block crystals were formed. After removing the glass vial from the oven and allowing it to cool to room temperature for about an hour without stirring, red block crystals were then separated by filtration and washed three times with methanol. The separated crystals were further immersed and exchanged 6 times every 24 hours in methanol before activating at 100 °C under a high vacuum for 12 hours to afforded **CPOC-107** with a yield of about 72%. ^{1}H NMR (400 MHz, $CDCl_3$, 298 K): δ 13.15 (s, 1H), 10.30 (s, 1H), 8.36 (s, 1H), 7.38 (s, 1H), 4.47 (t, 1H), 2.04 (t, 2H), 1.59 (s, 2H), 1.46 (m, 1H), 1.00 (d, 6H) p.p.m. HR-MS: $[M-2H]^{2-}$ calcd. for **CPOC-107** ($C_{116}H_{128}N_{32}O_{16}$) is 968.233; found 968.162.

Synthesis of CPOC-203: C4RACHO (0.05 mmol, 41 mg) and DTA (0.1 mmol, 9.9 mg) were dissolved in nitrobenzene/methanol 2:1 (3 mL). The mixture was sealed in a 10 mL glass vial, and put in an oven with a temperature of 100 °C for 72 hours without stirring, during which red block crystals were formed. After removing the glass vial from the oven and allowing it to cool to room temperature for about an hour without stirring, red block crystals were then separated by filtration and washed three times with methanol. The separated crystals were further immersed and exchanged 6 times every 24 hours in methanol before activating at 100 °C under a high vacuum for 12 hours to afforded **CPOC-203** with a yield of about 70%. ^{1}H NMR (400 MHz, $CDCl_3$, 298 K): δ 13.15 (s, 0.5H), 10.30 (s, 1H), 8.37 (s, 1H), 7.38 (s, 1H), 4.47 (t, 2H), 2.06 (t, 4H), 1.46 (m, 2H), 1.00 (d, 6H) p.p.m. HR-MS: $[M-3H]^{3-}$ calcd. for **CPOC-203** ($C_{156}H_{174}N_{30}O_{24}$) is 968.240; found 968.367.

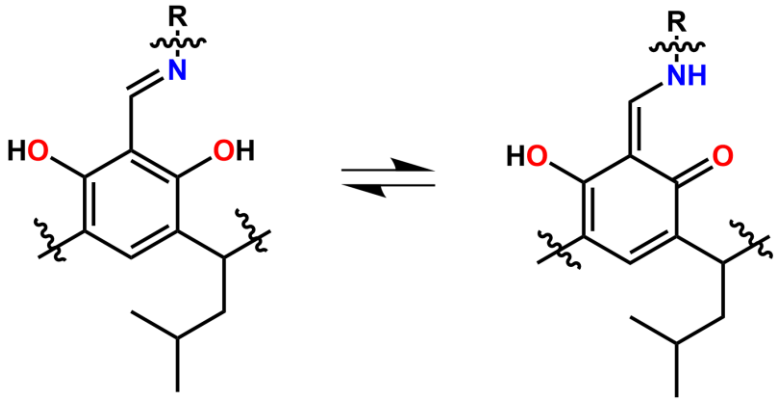

Fig. S1. Keto–enol tautomerization within **CPOC-107** and **CPOC-203**.

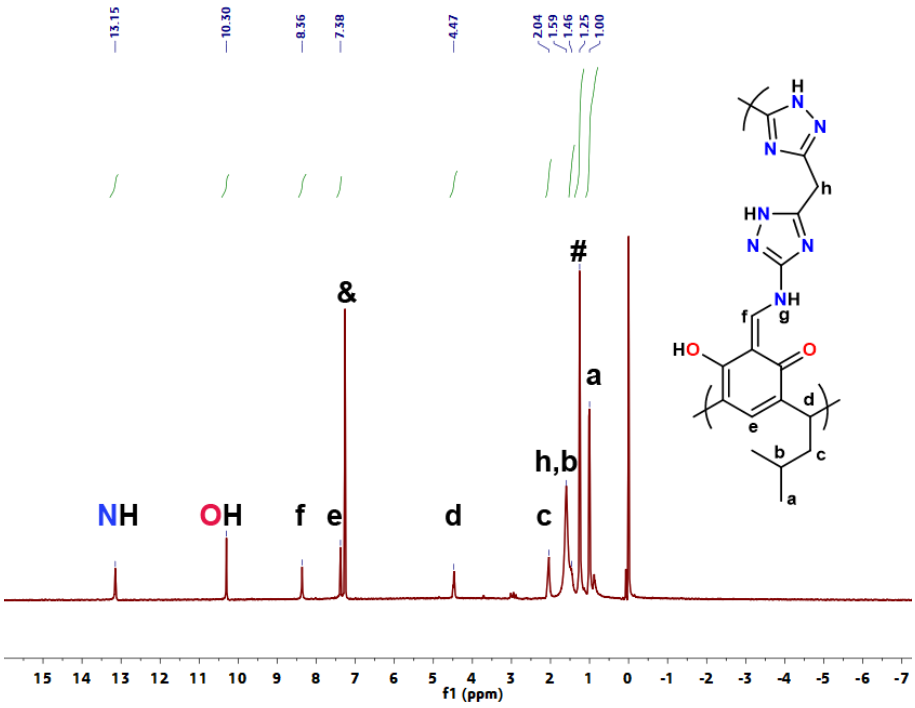

Fig. S2. ^{1}HNMR of **CPOC-107** ($CDCl_3$, 400 MHz, 298 K). The marked extra peaks：$^{\&}CHCl_3$, $^{\#}$Solvent impurity. The NH (g) signal was not observed in the solution state, likely due to that it is active hydrogen atom, and/or is mainly in enol form.

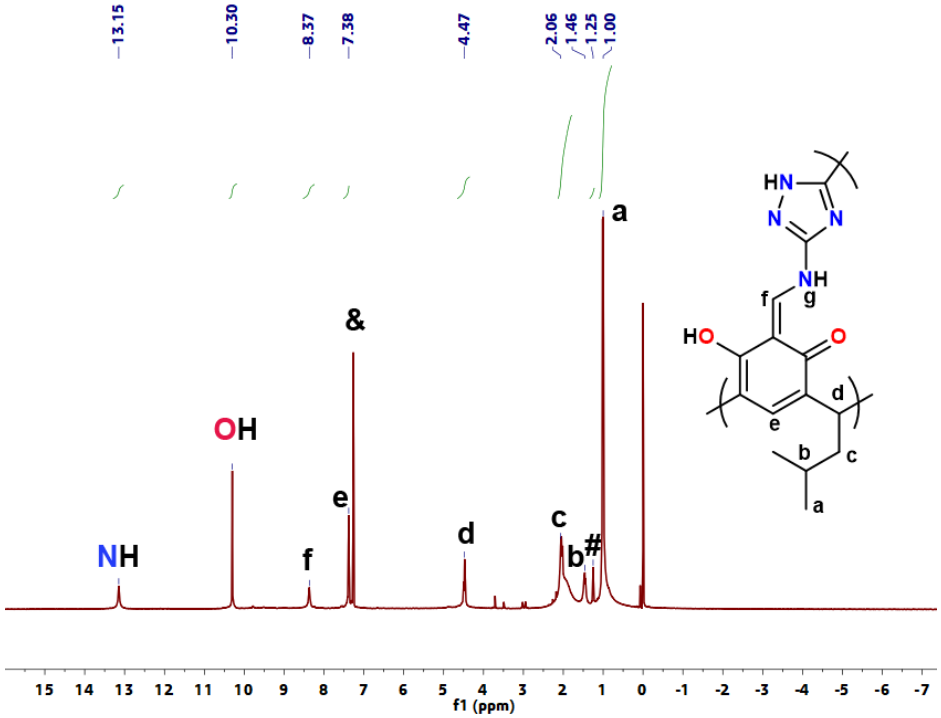

Fig. S3. ^{1}H NMR of **CPOC-203** ($CDCl_3$, 400 MHz, 298 K). The marked extra peaks：$^{\&}CHCl_3$, $^{\#}$Solvent impurity. The NH (g) signal was not observed in the solution state, likely due to that it is active hydrogen atom, and/or is mainly in enol form.

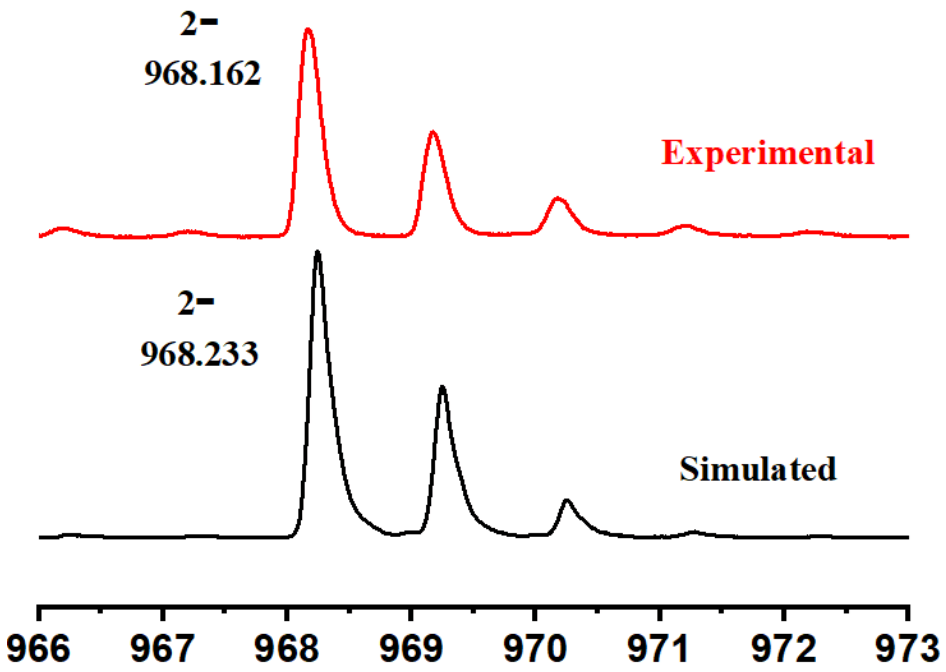

Fig. S4. HR-MS spectrum of **CPOC-107** recorded in $CHCl_3$.

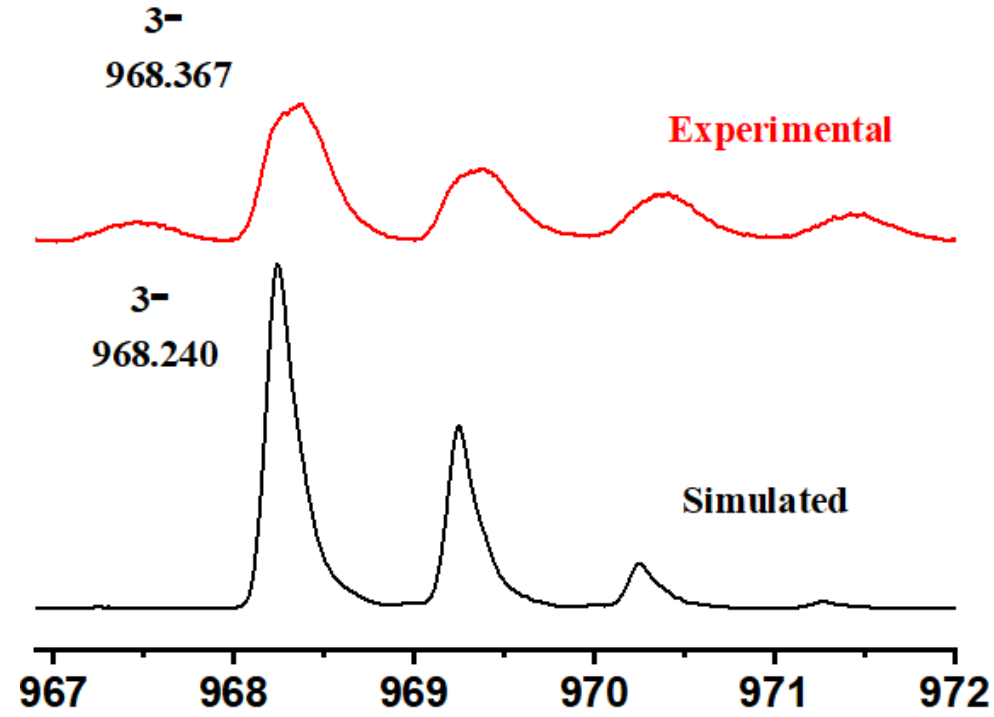

Fig. S5. HR-MS spectrum of **CPOC-203** recorded in $CHCl_3$.

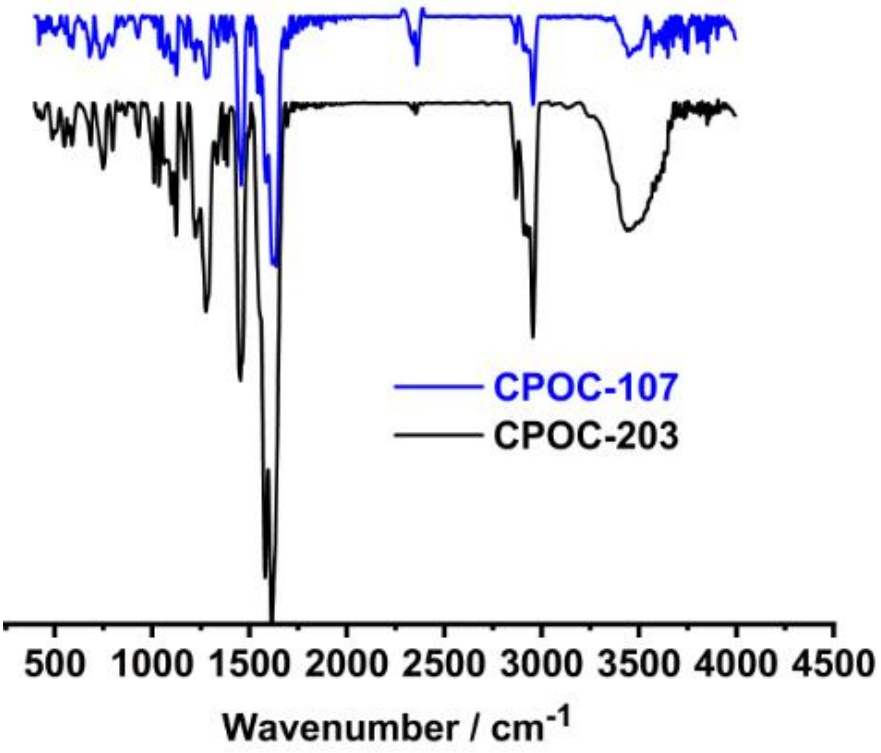

Fig. S6. FT-IR spectra of **CPOC-107** and **CPOC-203**.

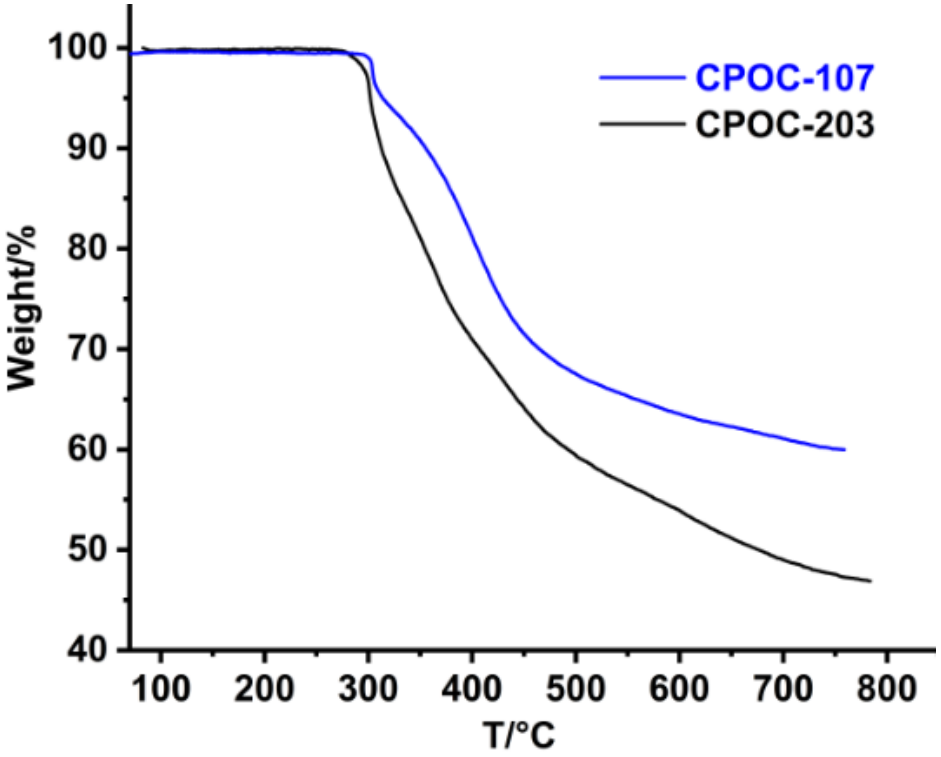

Fig. S7. TGA curves of **CPOC-107** and **CPOC-203**.

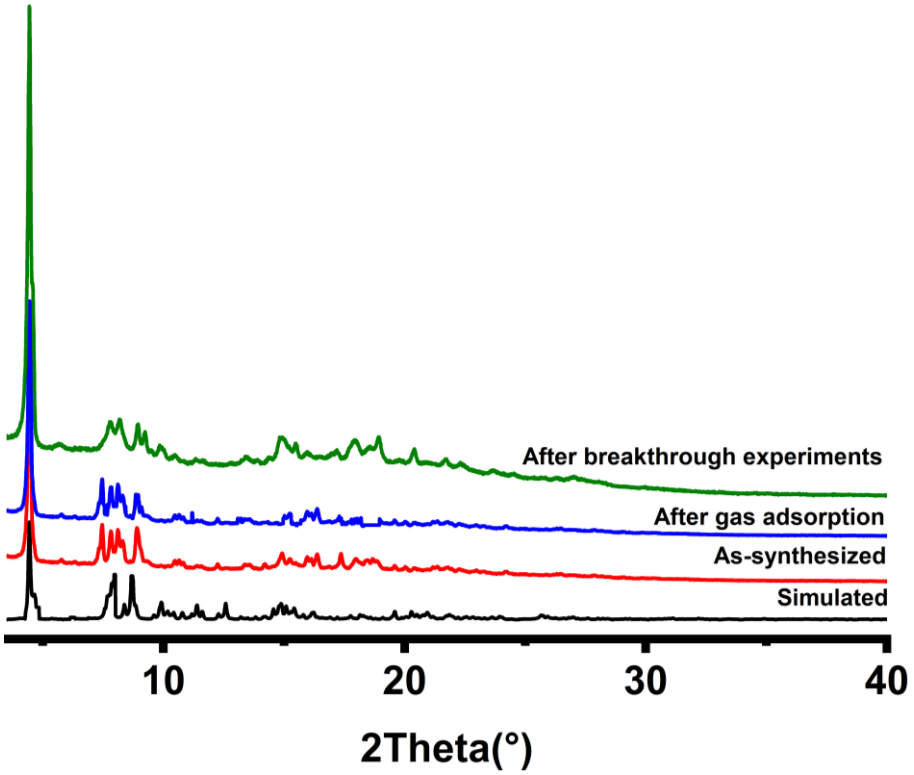

Fig. S8. PXRD curves of **CPOC-107**.

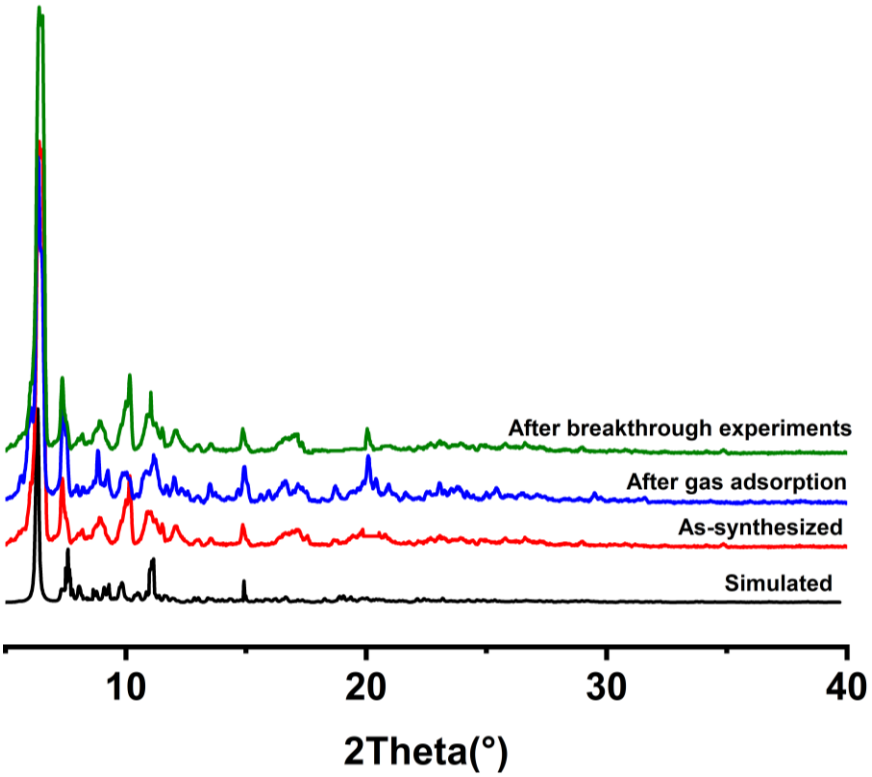

Fig. S9. PXRD curves of **CPOC-203**.

Section S3. X-ray Data Collection and Structure Determination

Single-Crystal X-ray Crystallography: Both X-ray single crystal data for **CPOC-107** and **CPOC-203** were collected on XtaLAB Synergy R, HyPix diffractometer equipped with PhotonJet R (Cu) X-ray source (λ = 1.5406 Å). The crystal structures were resolved by direct methods and all calculations were performed on the *SHELXTL*-2016 program package.[S7] All non-hydrogen atoms were refined anisotropically for the CPOCs. Hydrogen atoms of the organic ligands were added in the riding model and refined with isotropic thermal parameters. Moreover, the diffuse electron density together with highly disordered solvent molecules of crystallization could not be generated and were not included for both **CPOC-107** and **CPOC-203**, thus the crystal structures were treated by the "SQUEEZE" method,[S8] a part of the PLATON package of crystallographic software. This had dramatically improved the agreement indices. Moreover, the high R_1 and wR_2 factor for all **CPOC-107** and **CPOC-203** might be due to the weak crystal diffraction, the disorder of the isobutyl groups as well as no heavy atoms in the molecular structure, which are typical, especially for in organic cage system.[S9-11] The detail crystal data and cell parameters for **CPOC-107** and **CPOC-203** are summarized in Tables S1.

Table S1. Crystallographic Data and Structure Refinement for **CPOC-501** and **CPOC-502**

	CPOC-107	**CPOC-203**
Formula	$C_{116}H_{128}N_{32}O_{16}$	$C_{156}H_{174}N_{30}O_{24}$
M / g mol^{-1}	2226.50	2850.54
T / K	100	100
Crystal system	monoclinic	monoclinic
Space group	*P*-1	*P*-1
a / Å	16.7240(4)	18.4175(3)
b / Å	16.8793(4)	26.5954(4)
c / Å	33.1977(8)	26.6943(4)
α (°)	95.303(2)	60.796(2)
β (°)	102.508(2)	84.325(1)
γ (°)	102.390(2)	88.155(1)
V / Å^3	8840.5(4)	11355.5(4)
Z	2	2
μ (mm^{-1})	0.473	0.469
Data measured	103179	131382
Ind. reflns	29600	44991
Parameters	1494	1915
GOF on F^2	2.350	1.394
R_1[a] [I ›σ(I)]	0.1931	0.0830
wR_2[b]	0.5349	0.3103
CCDC number	2255900	2255901

[a]$R_1 = \sum||F_o| - |F_c||/\sum|F_o|$. [b]$wR_2 = \{\sum[w(F_o^2 - F_c^2)^2]/\sum[w(F_o^2)^2]\}^{1/2}$

Section S4. Gas Adsorption and Separation Measurements

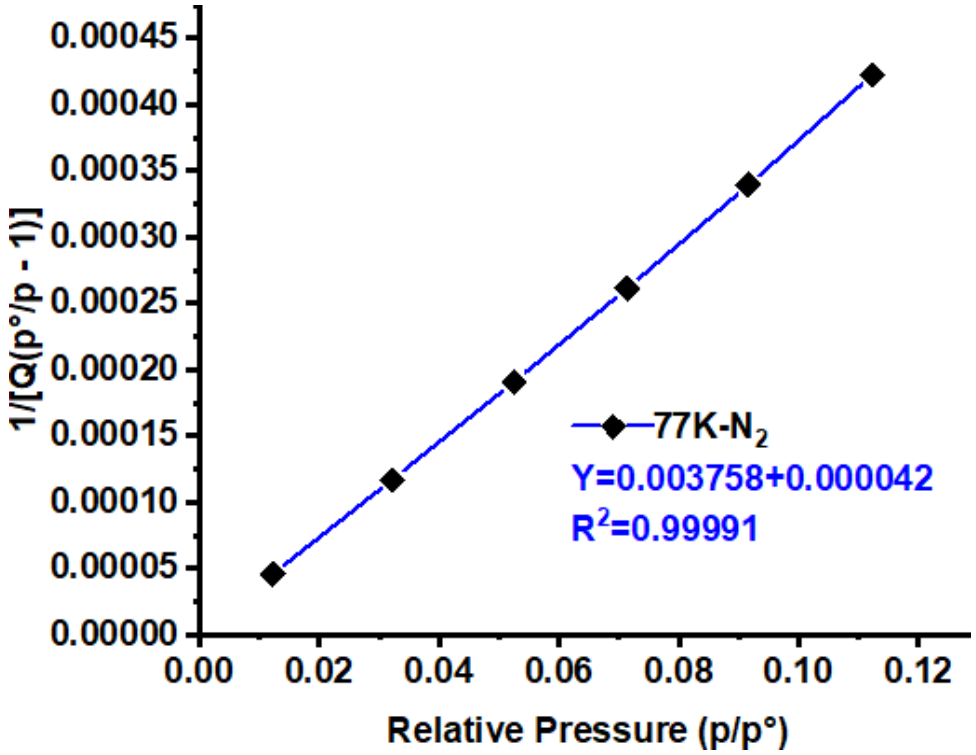

Fig. S10. BET-plots of **CPOC-107**.

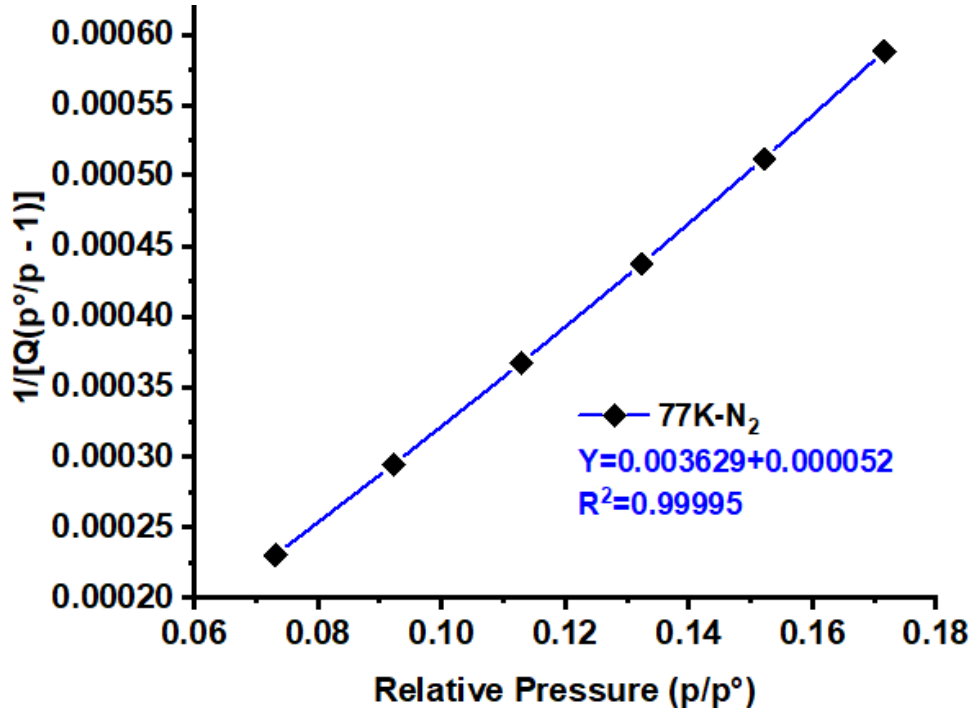

Fig. S11. BET-plots of **CPOC-203**.

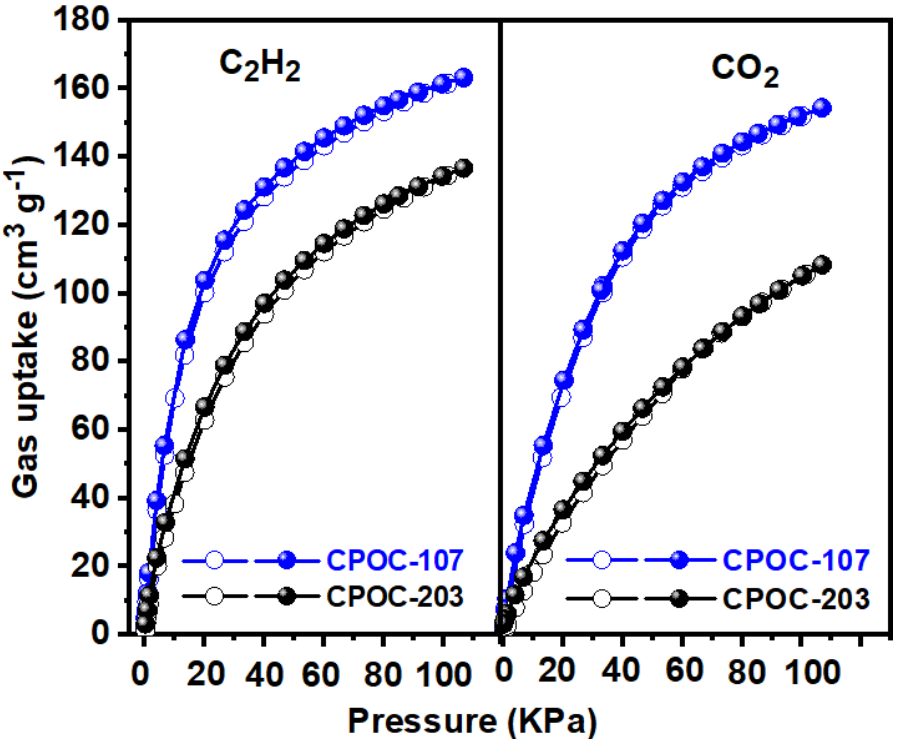

Fig. S12. C_2H_2 and CO_2 adsorption/desorption isotherm of **CPOC-107** and **CPOC-203** at 273 K.

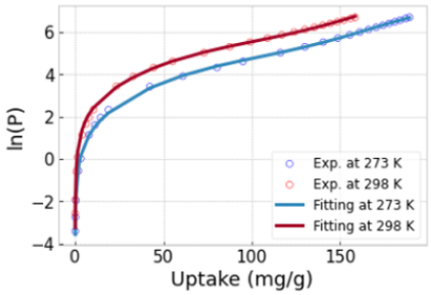

	Parameter Value	Standard Deviation
a_0	-3.323339e+03	2.528939e+02
a_1	1.308220e+01	1.037307e+01
a_2	4.857054e-03	1.172949e-01
a_3	-1.306895e-03	1.426925e-03
a_4	8.884552e-06	8.535472e-06
a_5	-1.899587e-08	1.809957e-08
Adj. R-Squared	0.9999	

Fig. S13. (a) Virial equation fitting of the C_2H_2 adsorption isotherm of **CPOC-107** at 273 and 298 K. (b) Relevant fitting parameters for C_2H_2.

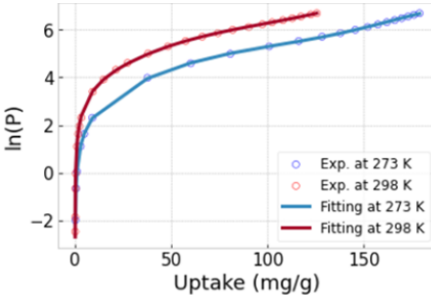

	Parameter Value	Standard Deviation
a_0	-3.732016e+03	9.968712e+02
a_1	1.227689e+01	5.196119e+00
a_2	2.850556e-02	5.651425e-02
a_3	-1.925275e-03	7.117711e-04
a_4	1.172010e-05	4.584571e-06
a_5	-2.404539e-08	1.039143e-08
Adj. R-Squared	0.9999	

Fig. S14. (a) Virial equation fitting of the C_2H_2 adsorption isotherm of **CPOC-203** at 273 and 298 K. (b) Relevant fitting parameters for C_2H_2.

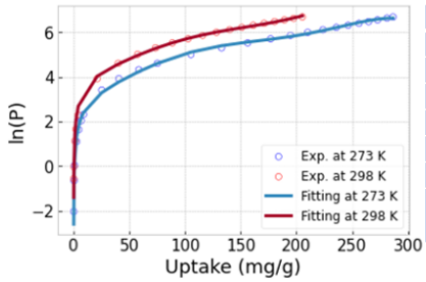

	Parameter Value	Standard Deviation
a_0	-3.173022e+03	3.954491e+02
a_1	1.106260e+01	1.131547e+01
a_2	9.356364e-02	7.780540e-02
a_3	-1.466156e-03	6.820810e-04
a_4	5.287516e-06	2.738289e-06
a_5	-6.810117e-09	3.868201e-09
Adj. R-Squared	0.9999	

Fig. S15. (a) Virial equation fitting of the CO_2 adsorption isotherm of **CPOC-107** at 273 and 298 K. (b) Relevant fitting parameters for CO_2.

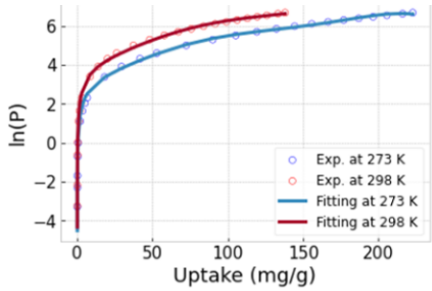

	Parameter Value	Standard Deviation
a_0	-2.399333e+03	4.421672e+02
a_1	-1.283848e+01	2.123699e+01
a_2	3.029764e-01	1.905924e-01
a_3	-3.028390e-03	1.757637e-03
a_4	1.395727e-05	9.338560e-06
a_5	-2.333134e-08	1.737743e-08
Adj. R-Squared	0.9999	

Fig. S16. (a) Virial equation fitting of the CO_2 adsorption isotherm of **CPOC-203** at 273 and 298 K. (b) Relevant fitting parameters for CO_2.

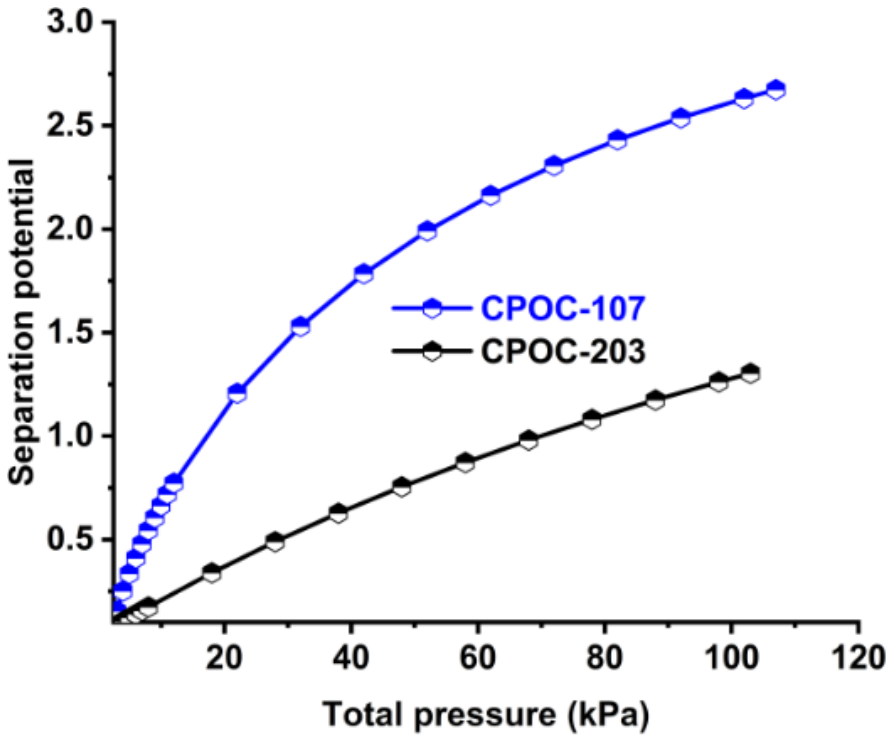

Fig. S17. Plots of the calculated separation potential Δq break in the fixed bed with the calculated separation potential Δq_{IAST} from the static adsorption isotherms for equimolar C_2H_2/CO_2 mixture for **CPOC-107** and **CPOC-203**.

Section S5. References

1. H. Li, B. Yan, H. Ma, Z. Sun, Y. Ma and Z. J. A. C. S. C. S. C. Zhang, *Acta Crystallogr. C.*, 2020, **76**, 64-68.
2. M. Grajda, M. Wierzbicki, P. Cmoch and A. Szumna, *J. Org. Chem.*, 2013, **78**, 11597-11601.
3. A. L. Myers and J. M. Prausnitz, *AlChE J.*, 1965, **11**, 121-122.
4. R. Krishna, *Rsc Adv.*, 2017, **7**, 35724-35737.
5. R. Krishna, *Acs Omega*, 2020, **5**, 16987-17004.
6. A. L. Myers and J. M. Prausnitz, *AICHE J.*, 1965, **11**, 121-122.
7. G. M. Sheldrick, *Acta Crystallogr. C.*, 2015, **71**, 3-8.
8. A. L. Spek, *Acta Crystallogr. C.*, 2015, **71**, 9-18.
9. K. E. Jelfs, X. Wu, M. Schmidtmann, J. T. A. Jones, J. E. Warren, D. J. Adams and A. I. Cooper, *Angew. Chem. Int. Ed.*, 2011, **50**, 10653-10656.
10. B. Teng, M. A. Little, T. Hasell, S. Y. Chong, K. E. Jelfs, R. Clowes, M. E. Briggs and A. I. Cooper, *Cryst. Growth Des.*, 2019, **19**, 3647-3651.
11. J. Koo, I. Kim, Y. Kim, D. Cho, I.-C. Hwang, R. D. Mukhopadhyay, H. Song, Y. H. Ko, A. Dhamija, H. Lee, W. Hwang, S. Kim, M.-H. Baik and K. Kim, *Chem*, 2020, **6**, 3374-3384.